HHS Public Access

Author manuscript

DNA Repair (Amst). Author manuscript; available in PMC 2024 May 24.

Published in final edited form as:

DNA Repair (Amst). 2022 August ; 116: 103344. doi:10.1016/j.dnarep.2022.103344.

The *ataxia-telangiectasia mutated* gene product regulates the cellular acid-labile sulfide fraction

Mohammad Z. Islam,

Xinggui Shen,

Sibile Pardue,

Christopher G. Kevil,

Rodney E. Shackelford*

Department of Pathology & Translational Pathobiology, LSU Health Sciences Center Shreveport, Shreveport, LA 71130, United States

Abstract

The *ataxia-telangiectasia mutated* (ATM) protein regulates cell cycle checkpoints, the cellular redox state, and double-stranded DNA break repair. ATM loss causes the disorder *ataxia-telangiectasia* (A-T), distinguished by ataxia, telangiectasias, dysregulated cellular redox and iron responses, and an increased cancer risk. We examined the sulfur pool in A-T cells, with and without an ATM expression vector. While free and bound sulfide levels were not changed with ATM expression, the acid-labile sulfide faction was significantly increased. ATM expression also increased cysteine desulfurase (NFS1), NFU1 iron-sulfur cluster scaffold homolog protein, and several mitochondrial complex I proteins' expression. Additionally, ATM expression suppressed cystathionine β-synthase and cystathionine γ-synthase protein expression, cystathionine γ-synthase enzymatic activity, and increased the reduced to oxidized glutathione ratio. This last observation is interesting, as dysregulated glutathione is implicated in A-T pathology. As ATM expression increases the expression of proteins central in initiating 2Fe-2S and 4Fe-4S cluster formation (NFS1 and NFU1, respectively), and the acid-labile sulfide faction is composed of sulfur incorporated into Fe-S clusters, our data indicates that ATM regulates aspects of Fe-S cluster biosynthesis, the transsulfuration pathway, and glutathione redox cycling. Thus, our data may explain some of the redox- and iron-related pathologies seen in A-T.

Keywords

ataxia-telangiectasia ; ATM; Hydrogen sulfide; Iron-sulfur cluster; NFS1; NFU1

*Corresponding author. RdnyShac@aol.com (R.E. Shackelford).

Authors' contributions

Drs. Islam, Shen, and Pardue carried out the experiments included in this manuscript. Drs. Kevil and Shackelford contributed to the planning, organization, and writing of the manuscript. Drs. Rashdan provided technical assistance and materials for this work.

Author statement

I would like to re-submit the article titled "The *ataxia-telangiectasia mutated* Gene Product Regulates the Cellular Acid-Labile Sulfide Fraction" All the authors agree with the contents of the manuscript and there are no conflicts of interest. Additionally, I have answered all of the reviewer's questions to the best of my ability.

Conflicts of Interest

No relevant conflicts of interest to declare.

1. Introduction

The *ataxia-telangiectasia mutated* (ATM) gene is located on chromosomal region 11q22.3–23.1 and encodes a 350 kDA protein belonging to the phosphatidylinositol 3-kinase-related protein kinase family (PIKK) [1]. The PIKK family proteins were identified by DNA sequence analysis and include the mammalian target of rapamycin, ATM, suppressor of morphogenesis in genitalia, DNA-dependent protein kinase, transformation/transcription domain-associated protein, and the ATM and Rad-3-related protein kinase (ATR) [1-3]. ATM phosphorylates over 700 proteins, preferentially phosphorylating threonine or serine residues followed by a glutamine [4,5]. ATM is activated by multiple stimuli; with oxidative stress and double-stranded DNA (dsDNA) break responses being well characterized [1-4]. Following dsDNA break formation, ATM binds to the dsDNA breaks in an Mre11-Rad50-NBS1 protein complex-mediated process, where it then phosphorylates multiple substrates, initiates cell cycle checkpoints, and participates in homologous recombination DNA repair [3-5]. ATM loss results in the autosomal recessive disease *ataxia-telangiectasia* (A-T), distinguished by cerebellar Purkinje and granular cell death causing progressive ataxia, oculocutaneous telangiectasias, elevated cellular reactive oxygen species (ROS) production, dysregulated redox homeostasis, immunodeficiency, oxidant and ionizing radiation hypersensitivities, and an elevated cancer risk [3-6]. Interestingly, compared to ATM wild-type cells, A-T cells also show dysregulated iron responses, with iron chelators and iron-free media increasing A-T cell colony formation and oxidative-stress resistance, while lowering oxidative stress-induced dsDNA breaks. Conversely, low 1–3 nM labile iron concentrations inhibit A-T cell growth and increase dsDNA breaks; effects not seen in wild-type cells or in A-T cells carrying an ATM expression vector [7-10]. Interestingly, *Atm*-deficient mice also show increased serum and hepatic iron, with higher ferritin and hepcidin levels [11].

Hydrogen sulfide (H_2S) is a gasotransmitter that functions in many different cellular processes, including redox regulation [12-15]. H_2S is synthesized by cystathione γ-synthase (CBS), cystathione γ-lyase (CSE), and 3-mercaptopyruvate sulfurtransferase (3-MST) [13-18]. Within cells H_2S occurs as free H_2S, protein-bound sulfane sulfur, and acid-labile sulfide fractions (ALS) [16-18]. The ALS is made up of sulfur present in iron-sulfur (Fe-S) clusters contained in abundant non-heme Fe-S cluster proteins [16-19]. The ALS fraction was first identified in the brain, is predominantly mitochondrial, and includes succinate dehydrogenase, aconitase, rubredoxins, ferredoxins, and many proteins involved in oxidative phosphorylation [16-19]. Relatively little is known about how the ALS fraction is regulated, although interestingly, it is low in cardiovascular disease [16]. The sulfane or bound sulfur fraction is composed of sulfur attached solely to other sulfur atoms and includes elemental sulfur S^0, R-S-SH, thiosulfonates R-S(O)-S-R', persulfides, thiosulfate $S_2O_3^{2-}$, polythionates $S_nO_6^{2-}$, and polysulfides R-S_n-R [16-18]. Recently, we found that the ATR kinase regulates cellular H_2S concentrations, while H_2S in turn modulates CHK1 phosphorylation by ATR and ATR serine 435 phosphorylation, an event correlating with ATR kinase activation and nucleotide excision repair capacity [15,20].

The PIKK gene family members show extensive homology, with ATM and ATR exhibiting many partially overlapping substrate specificities and functions [2,3,21,22]. Interestingly,

A-T cells also show dysfunctional glutathione homeostasis, and *Atm*-deficient mice and A-T patients exhibit lower cystine/glutamate exchanger subunit xCT, glutathione-S-transferase, glutathione reductase, glutathione peroxidase activity, and glutathione in their cerebellar astroglia, indicating that ATM plays a major role maintaining the cellular redox balance and its loss can contribute to disease [23-25]. Thus, some aspects of both sulfur and iron metabolism are dysregulated in A-T [7-11,23-25]. Here we hypothesize that the ATM kinase functions in cellular sulfur pool regulation and this regulation in turn, is related to iron metabolism.

2. Methods and materials

2.1. Materials

Colcemid, sulfosalicylic acid (SSA), 1-fluoro-2,4-dinitrobenzene (DNFB), monobromobimane (MBB), ninhydrin, Tris (2-carboxyethyl) phosphine hydrochloride (TCEP), diethylenetriamine pentaacetate (DTPA), TPP® tissue culture dishes, *t*-butyl hydroperoxide (*t*-BOOH), penicillin/streptomycin, pyridoxal 5'-phosphate, and cystathione were from Sigma (St. Louis, MO). pLPCX cyto Grx1-roGFP2 was from Adgene (Watertown, MA). FLUOstar Optima was from BMG Labtech (Offenburg, Germany). Dulbecco's modified Eagle's medium (DMEM, standard liquid media), Lipofectamine 2000, and fetal bovine serum, were purchased from Invitrogen (Rockville, MD). The antibodies employed were anti-CBS (catalog number sc-67154, Santa Cruz Biotechnology), anti-CSE (catalog number sc-101924, Santa Cruz Biotechnology), anti-3-MST (catalog number sc-135993, Santa Cruz Biotechnology, Santa Cruz, CA), and anti-beta-actin (catalog number ab8227, abcam). The secondary antibodies employed were HRP conjugated anti mouse IgG (#7076) and HRP conjugated anti-Rabbit IgG (#7074) purchased from Cell Signaling Technology (Danvers, MA).

2.2. Cells

The AT22 cell line is an ATM-deficient SV-40 immortalized fibroblast cell line, originally established from primary A-T fibroblasts. These cells were transduced with a hygromycin resistance expression vector, AT22IJE-T pEBS7 or "ATM(−/−)" cells, or a combined hygromycin resistance and ATM expression vector, AT22IJE-T pEBS7-YZ5 or "ATM(+/+)" cells. The cells were cultured in DMEM with 100 μg/ml hygromycin, 1% penicillin/streptomycin, and 5% FBS [26]. Only low-passage AT22IJE-T pEBS7 and AT22IJE-T pEBS7-YZ5 cells, at three or fewer 1: 4 splittings, were used in all experiments. Additionally, the ATM vector-corrected/AT22IJE-T pEBS7-YZ5 cells were monitored for ATM protein expression by western blot analyses in all experiments. WI-38 VA13 (VA13) is an SV-40-immortalized ATM wild-type fibroblast cell line (ATCC, Rockville, MD) [26,27]. The VA13 and AT22 cells line were cultured in 1% penicillin/streptomycin, and 5% FBS [7-11,26].

2.3. H_2S measurements

Cell lysates were analyzed for the free (H_2S), ALS, bound (BSS), and total sulfide fractions by the MBB method [16-18,20]. Free H_2S was measured using 30 μl of cell extract with MBB; whereas for ALS and BSS detection, 30 μl of cell extract was separately added

into two 4 ml BD vacutainer tube sets. Four hundred and fifty μls of pH 2.6 100 mM phosphate buffer containing 0.1 mM DTPA was added to a tube for the ALS reaction and 450 μl of 100 mM phosphate buffer (pH 2.6, 0.1 mM DTPA) with 1 mM TCEP (Tris(2-carboxyethyl)phosphine) was added to a second tube for the total sulfide measurement. Following 30 min on a nutator, the reaction liquid was removed, with the evolved sulfide gas trapped by the addition 500 μl of 100 mM Tris-HCl buffer (pH 9.5, 0.1 mM DTPA) into the BD vacutainer tube, subsequently followed by 30 min on a nutator mixer. Upon trapping solution removal, the sulfide levels were measured by the MBB method [16-18,20]. ALS determination was achieved through reacting the cell lysates with acidic phosphate buffer alone, followed by evolved sulfide trapping. BSS measurement was obtained by subtracting the ALS value from the total sulfide protocol with TCEP reductant treatment in acidic conditions. Total sulfide levels were drawn from the total sulfide reaction. All sulfur fraction assays were performed in triplicate.

2.4. Mass spectrophotometry

ATM(−/−) and ATM(+/+) cells were collected and lysed by Thermo Scientific™ EasyPep™ Lysis Buffer. Protein concentrations were estimated using a BCA assay. Protein (10 μg) from each sample was trypsin digested followed by disulfide bond reduction with dithiothreitol and cysteine alkylation with iodoacetamide, by the manufacturer's protocol for the Thermo Scientific™ In-Solution Tryptic Digestion kit. The digested peptides were vacuum-dried and resolved in the LC/MS grade water containing 0.1% (v/v) formic acid, followed by untargeted discovery proteomics analysis. This LC-MS/MS analysis was performed with an Ultimate 3000 RSLCnano system coupled to an Orbitrap Exploris 480 mass spectrometer. The digested peptides (1.0 μl) were placed in a trap column (PepMap C18, 2 cm × 100 μm, 100 Å) at a of 20 μl/min flow rate, using 0.1% formic acid, and resolved on an analytical column (EasySpray 50 cm × 75 μm, C18 1.9 μm, 100 Å) with a 300 nl/min flow rate with a linear gradient of 5–45% solvent B (100% ACN, 0.1% formic acid) over a 120 min gradient. Precursor and fragment ions were obtained in the Orbitrap mass analyzer. Precursor ions acquisition was in an *m/z* range of 375–1500, with resolution at 120,000 (at *m/z* 200). Precursor fragmentation was performed by the higher-energy collisional dissociation method employing normalized collision energy (NCE) of 32. Fragment ions were obtained at a 150,000 resolution (at *m/z* 200). Scans were arranged by top-speed method, with a 3 s cycle time between MS and MS/MS. Ion transfer capillary voltage was maintained at 2.1 kV. Raw mass spectrometric data was interrogated by Proteome Discover (version 2.5, Thermo Fisher Scientific) software package with SequestHT employing species-specific fasta database and the Percolator peptide validator. Cysteine alkylation was placed as a fixed modification. Deamidation and acetylation of protein N-termini, Met oxidation, and Asn deamidation were selected as variable modifications. Differential iron protein and cysteine desulfurase were screened from the identified proteins and protein-protein interaction networks were analyzed by using String online tool (version 11.5).

2.5. CSE enzymatic assay

Cells were lysed and incubated with 2 mM cystathione and 0.25 mM pyridoxal 5'-phosphate with 100 mM pH 8.3 Tris-Hcl buffer at 37 °C for 30 min. Twenty percent trichloroacetic acid was then placed in the reaction mixture. Following centrifugation, 2% ninhydrin

reagent was mixed into the supernatant, incubated 5 min at 105 °C, and quick cooled to 4 °C. Samples were then mixed with 97% ethanol and read at 455 nm employing a spectrophotometer (Biotek). CSE activity was analyzed by cystathione consumption and enzyme activity given as fold change calculated from nanomoles consumed per mg of total protein [27]. All CSE enzymatic assays were performed in triplicate.

2.6. Western blotting

ATM(−/−) and ATM(+/+) cells were grown in 6-well plates and upon media removal and washing, the cells were lysed with 300 μl of SDS sample buffer (62.5 mM Tris-HCl [pH 6.8], 2% w/v SDS, 10% glycerol, 50 mM dithiothreitol, 0.1% w/v bromphenol blue) added per well. The lysates were harvested by cell scraping and placed into Eppendorf tubes. The lysates were boiled, centrifuged, and frozen at − 20 °C until gel the electrophoresis analysis. The lysates were separated by SDS-PAGE, transferred to polyvinylidene difluoride membranes. Next 5% nonfat dry milk was used to block the membranes, followed by the addition of primary antibodies. Densitometry was performed by Image Lab 6.0.1 software (Bio-Rad) [20]. All western blots were performed in triplicate.

2.7. Quantitative real-time polymerase chain reaction

PCR reactions were done as previously describes [20]. ATM(−/−) and ATM(+/+) cell total RNA was collected using Trizol per the manufacturer instructions. RNA (1 μg) was reverse transcribed using an iScript cDNA synthesis kit (1708891, Bio-rad). Quantitative real-time PCR was done using SYBR Green Master Mix (Bio-rad, 1708882) with gene expression quantified through the $2^{-\Delta\Delta CT}$ method. The genes examined were normalized to GAPDH. The PCR primers employed here are in Table 1. These assays were performed in triplicate.

2.8. Cellular glutathione: oxidized glutathione ratio (GSH: GSSG)

ATM(−/−) and ATM(+/+) cells were cultured in Advanced DMEM with 5% heat inactivated FBS, 100 U/ml penicillin, 2 mM L-glutamine, and 100 mg/ml streptomycin. Cells were plated in a clear bottom 96 well black plate at 0.5×10^5 cells/well, resulting in confluence the next day of around 90%. The cells were transfected with 0.2 ug/well of pLPCX cyto Grx1-roGFP2 plasmid using Lipofectamine 2000 transfection reagent following standard protocol. pLPCX cyto Grx1-roGFP2 was a gift from Tobias Dick (Addgene plasmid # 64975: http://n2t.net/addgene:64975;RRID:Addgene_64975) [62]. After 24 hr, the media was changed and the ro-GFP2 redox state was measured at 510 nm emission after excitation at 395 and 480 nm in plate reader. The GSH: GSSG ratio was obtained by calculating the ratio of emission (395/480 nm). These assays were performed in triplicate.

2.9. Chromosomal preparation and analysis

Chromosomal dsDNA breaks in the ATM(−/−) and ATM(+/+) cells were analyzed as previously described [20]. Each treatment consisted of ATM(−/−) and ATM(+/+) cells at 50% confluence treated 15 min with 10 μM *t*-BOOH and washed with PBS 3X. The media was replaced, and the cells were incubated for 1 hr. Following this, 100 ng/ml colcemid was added for 4 hr and the cells were by washed 2X with PBS, trypsinized, and placed in a 15 ml tube. Next 2 ml of DMEM containing 5% FBS was placed in the tubes, with

the cells subsequently pelleted at 500 x *g* for 5 min. The cells were next re-suspended in 5 ml 0.075 mM KCl, incubated 37 °C for 15 min, and 200 μl of fresh 3:1 methanol: glacial acetic acid (Carnoy's fixative) was added, followed by gentle vortexing, and pelleting at 500 x g for 5 min. The supernatant was next removed, Carnoy's fixative (5 ml) was added with gentle vortexing, the cells pelleted at 500 x *g* for 5 min, the supernatant again removed, and 5 ml more of Carnoy's fixative was added with gentle vortexing. The final chromosomal preparations were made following pelleting at 500 x *g* for 5 min, supernatant removal, dropping on slides, 30 min at 90 °C drying, Giemsa staining, washing, and finally cover-slipping. Per data point, 5000 chromosomal observations performed by oil immersion microscopy in triplicate. Only the most obvious and clear dsDNA breaks were counted. An example is shown in an insert in Fig. 5.

2.10. Statistical analysis

The experimental statistical significances in this paper were calculated by paired t-test or ANOVA by using Microsoft Excel or Prism software version 5.02 prism (GraphPad Inc., San Diego, CA). The *P* values are shown in the figures. The standard error of the mean (SEM) was calculated by using the standard deviation for the sulfide fractions or dsDNA breaks and dividing this number by the square root of the sample size [20].

3. Results

3.1. ATM protein expression in A-T cells significantly increases the cellular ALS/Fe-S cluster faction

To initiate these studies, we compared the free H_2S, ALS, BSS, and the total sulfide faction levels in immortalized A-T fibroblasts, without and with ATM an expression vector [26]. As shown in Fig. 1, the H_2S, BSS, and total sulfide cellular fractions were not significantly different with ATM expression. However, the ALS fraction was significantly (~9X) increased in the ATM(+/+) cells compared to the ATM(−/−) cells. As.

vector transduced ATM can undergo rearrangements, these experiments were repeated with the AT22 A-T cells line and the ATM wild-type pulmonary fibroblast VA13 cell line [7-11,26]. As shown in Fig. 1, comparison of the AT22 and VA13 cells revealed unchanged free H_2S, BSS, and total sulfide levels, while the ALS was significantly increased in the ATM wild-type cells (Fig. 1). Thus, the ALS fraction change seen with ATM expression in the ATM(−/−) cells is also seen in ATM wild-type cells compared AT22 A-T cell line. The sulfide fraction measurements for these experiments and the SEMs are given in Table 2. The parental AT22 cell line and VA13 cell line data is shown separately from the AT22IJE-T pEBS7, to avoid possible confounding effects of the hygromycin expression vector.

3.2. ATM expression in A-T cells increases cysteine desulfurase/mitochondrial NFS1 mRNA and NSF1 and NFU1 protein expression

Our data suggests that ATM expression increases the Fe-S cluster assembly protein expression. To test this hypothesis NFS1 mRNA levels were compared by PCR analysis between the ATM(−/−) and ATM(+/+) cells. NFS1 initiates Fe-S complex synthesis by transferring a cysteine sulfur to an NFS1 cysteine residue, forming a persulfide, which in

turn is transferred to the ISCU2 scaffold protein for initial Fe-S cluster assembly [28]. As shown in Fig 2A, NFS1 mRNA levels were significantly higher in the ATM(+/+) cells.

To examine ATM-related Fe-S cluster protein synthesis and metabolism-related protein expression more broadly, we employed mass spectrophotometric analysis to compare the two cell types. As shown is Fig. 2B and C, mass spectrophotometric analysis comparing the ATM (−/−) and ATM(+/+) cells revealed significantly increased NFS1, NFU1, NADH dehydrogenase Fe-S proteins 2, 7, and 8, (NDUFS2, −7, and −8) and succinate dehydrogenase with ATM expression. Conversely, slightly higher NADH dehydrogenase Fe-S protein 3 (NDUFS3) and CDGSH Fe-S domain-containing protein 1 (mitoNEET/CISD1), and much higher CDGSH Fe-S domain-containing protein 2 (CISD2) were seen in the ATM (−/−) cells compare to the ATM(+/+) cells (Fig. 2B). The protein-protein interaction of Fe-S proteins and cysteine desulfurase were analyzed using STRING and Cytoscape databases and are shown in Fig. 2C.

3.3. CBS and CSE mRNA and protein levels are higher in ATM(−/−) cells compared to ATM(+/+) cells and ATM expression suppresses CSE enzymatic activity

To ascertain if ATM plays a role in H_2S synthesizing enzyme expression, we performed PCR and western blot analyses for CSE, CBS, and 3-MST mRNA, and protein levels in the ATM(−/−) and ATM(+/+) cells. As shown in Fig. 3A, CBS and CSE mRNA expression were both elevated in the ATM(−/−) cells compared to the ATM(+/+) cells, while 3-MST mRNA expression was the same between the two cell types. Similarly, CBS and CSE protein expression was higher in the ATM(−/−) cells compared to the ATM(+/+) cells, while 3-MST protein levels were similar (Fig. 3B). Thus, the ATM protein expression functions as a negative regulator of CBS and CSE mRNA and protein expression, but not for 3-MST. Interestingly, the CBS protein migrated as two bands, with the lower band predominant in the ATM(−/−) cells and the upper band predominant in the ATM(+/+) cells (Fig. 3C, expanded CBS blot).

Since the mRNA and protein expression of CBS and CSE were different with cellular ATM expression, we compared CSE enzymatic activity without and with cellular ATM expression. CSE activity was higher in the ATM(−/−) cells compared to the ATM(+/+)cells, indicating that ATM is a negative regulator of CSE enzymatic activity (Fig. 3D). As previously found, ATM protein expression was seen in the ATM(+/+) cells and migrated at the same molecular weight as wild-type ATM [Fig. 3B, 7-10,26].

3.4. ATM expression increases the cellular GSH: GSSG in A-T cells

Atm-deficient mice show low astroglial cerebellar GSH and cysteine, with low glutathione reductase, cystine/glutamate exchanger subunit xCT, and glutathione-S-transferase levels, resulting in impaired cerebellar astroglial cell survival [24]. Additionally, low mitochondrial GSH levels result in lower Fe-S cluster proteins stabilities and activities, suggesting that the ATM-mediated increases in cellular Fe-S clusters may be accompanied by improvements in the cellular GSH profile [29]. To test this, we examined the ratio of GSH to GSSG in the ATM(−/−) and ATM(+/+) cells. As shown in Fig. 4, ATM expression significantly increased the cellular GSH: GSSG ratio, demonstrating that the ATM protein regulates GSH reduction.

3.5. N-acetyl-L-cysteine treatment decreases oxidative-stress mediated dsDNA breaks in A-T cells

Previously oxidative stress was found to increase A-T cell dsDNA breaks, an event partially inhibited with iron chelator co-treatment [7-10]. Additionally, N-acetyl-L-cysteine (NAC) treatment decreases genomic rearrangements in *Atm*-deficient mice, restores GSH concentrations in A-T mutant astroglia, and sustains cellular GSH levels in ATM wild-type cells [24,30,31]. Based on this, we hypothesized that NAC treatment would pharmacologically reduce oxidative stress-initiated dsDNA breaks in ATM(−/−) cells, in part, through its established effects on increasing cellular GSH levels. As shown in Fig. 5, compared to the ATM(+/+) cells, the ATM(−/−) cells showed higher oxidative stress-induced dsDNA breaks, which were suppressed by NAC treatment. Interestingly, NAC treatment did not significantly alter oxidative stress-induced dsDNA break levels in the ATM(+/+) cells, showing an effect unique to ATM loss. We measured dsDNA breaks formation by oil immersion microscopy, as many assays used to analyze cellular dsDNA breaks depend on ATM protein expression and thus would not be useful in A-T cells [6,20]. The exact dsDNA beak counts, and the standard error of the mean (SEM) are given in Table 3.

4. Discussion

Fe-S clusters are ubiquitous inorganic cofactors which facilitate electron transfer reactions and are found in approximately 1% of eukaryotic cell proteins [28]. Their synthesis is highly conserved in eukaryotes, comprising structurally and functionally diverse polynuclear combinations of iron and sulfur, serving as versatile biochemical cofactors, regulating processes including DNA replication and repair, transcriptional regulation, RNA modification, metabolite biosynthesis, viral resistance, and bioenergetic processes [28,32]. Here we found that the ALS fraction is low in the ATM(−/−) cells and is significantly increased in the ATM(+/+) cells, indicating a role for ATM in ALS fraction formation [16-19]. These cells were employed to allow the effects of ATM expression to be analyzed on the same genetic background. These findings were further confirmed by comparing the A-T AT22 cell line to the ATM wild-type VA13 cell line.

Previously, iron chelators were found to increase A-T cell viability and genomic stability [7-10]. Interestingly, ATM ablation in a breast cancer cell line increased the expression of the iron binding protein ferritin [33]. Combined with the data presented here, these previous findings suggest that cells compensate for the lower Fe-S cluster levels following ATM loss by increasing ferritin levels to maintain cellular iron homeostasis and cell viability. Thus, exogenous iron chelators may exert beneficial effects through a similar mechanism, explaining previous findings where iron chelator treatment increased the colony forming abilities and genomic stability of A-T, but not wild-type cells [7-10].

Mass spectrophotometric analysis revealed significantly increased NFS1 and NFU1 protein expression with ATM expression. The NFS1/mitochondrial cysteine desulfurase belongs to the pyridoxal 5′-phosphate-dependent transaminase subfamily and catalyzes the first step in *de novo* Fe-S cluster assembly by transferring a cysteine to alanine, forming a persulfide, that is transferred to the Fe-S cluster assembly scaffold proteins (ISCU) for complete 2Fe-2S cluster assembly [28,34]. NFS1 knockdown in HeLa cells results in

growth retardation, mitochondrial morphologic changes, and lowered activity of the Fe-S cluster enzymes succinate dehydrogenase and aconitase [34]. Human NFS1 mutations result in mitochondrial complex deficiencies, often with concomitant lactic acidemia and early age multisystem organ failure [35,36]. NFU1 catalyzes the assembly and transfer of 4Fe-4S clusters to target apoproteins, including lipoic acid synthase, the pyruvate dehydrogenase complex, and succinate dehydrogenase [28,34,37]. Rare NFU1 mutations result in a fatal infantile encephalopathy and/or possible pulmonary hypertension with lactic acidosis and hyperglycemia, leading to death before the age of 15 months [37]. Since NFS1 and NFU1 play important roles in Fe-S cluster synthesis, assembly, and processing, our data demonstrates a function for ATM in the regulation of proteins involved in Fe-S cluster synthesis [28,32,34-37]. Support for this is highlighted by the increased succinate dehydrogenase expression seen here with ATM expression, as this enzyme requires both proteins for its synthesis and expression [32,34-37]. The mechanism(s) by which ATM regulates NFS1 and NFU1 are unknown. However, both genes have promoter RUNX1/AML1a binding sites [38]. RUNX1 is also positively regulated by hypoxia-inducible factor-1α, which is dysregulated and low in A-T cells, suggesting that altered A-T cell hypoxia-inducible factor-1α activity may impinge of Fe-S cluster synthesis though NFS1 and NFU1 dysregulation [39,40].

The mitochondrial complex I proteins NDUFS2, − 7, and − 8 were also low in ATM(−/−) cells and increased in the ATM(+/+) cells. These Fe-S cluster proteins are vital for complex I catalytic activity and ATM inhibition within isolated cardiomyocytes causes rapid mitochondrial complex I activity inhibition [41-44]. Additionally, compared to wild-type mice, *Atm*-deficient mice show deficient complex I electron transport chain activity, an event which increases mitochondrially generated ROS [41-46]. Thus, our data is congruent with previous findings and partially explains both the mitochondrial dysfunction seen in A-T and the increased mitochondrially generated ROS levels [1,6,45]. Lastly, all four of the ATM-regulated Fe-S cluster complex I proteins we identified (NDUFS2, −3, −7, and −8) function together in early complex I assembly and are among the 14 of 45 complex I mitochondrial proteins essential for complex I activity [46]. The significance of this observation is unknown, although it suggests a conserved evolutionary relationship between ATM and mitochondrial function.

The reason why NDUFS3, CISD1/MitoNEET, and CISD2 expression are lower with ATM expression is not known. It is interesting that the proteins increased with ATM expression (NDUF2, −7, −8, and succinate dehydrogenase) contain 4Fe-2S clusters, while NDUFS3, CISD2, and CISD1/MitoNEET contain 2Fe-2S clusters [32,47-54]. As NFS1 is required to synthesize 2Fe-2S clusters, which are subsequently incorporated into 4Fe-4S clusters by an NFU1-dependent mechanism, these findings suggest that combined low ATM(−/−) cell NFS1 and NFU1 expression creates a biosynthetic “bottleneck” that significantly lowers cellular capacity for 4Fe-4S cluster synthesis [32,34-37]. ATM also regulates many transcription factors, such as ZEB1, ENL, and p53 [1-6, 55,56]. The differential regulation of these Fe-S cluster proteins may also be in part due to promoter sequences which bind different transcription factor sets. Further studies will be needed to examine these hypotheses. Support for Fe-S cluster loss in effecting the A-T phenotype comes from the observation that Fe-S cluster loss causes hepatocyte metabolic reprogramming with

concomitant lipid droplet formation [57]. In a study of 67 A-T patients ages 1–38, divided into two groups of under and over age 12, analyses revealed significantly higher hepatic steatosis, plasma liver enzymes, and ataxia as measured by the Klockgether Ataxia Score in the older patient group [58]. Our findings here suggest that poor Fe-S cluster formation may underlie these hepatic effects seen in A-T.

Our finding that ATM expression decreased CBS and CSE mRNA and protein expression, and lowered CSE enzymatic demonstrates a role for ATM transsufuluration pathway regulation. While CSE protein levels were approximately four times lower in the ATM(+/+) cells, CSE enzymatic activity was roughly 40% lower with ATM expression. The reason for this is unknown although it is likely at ATM-dependent post-translational medications on CSE are playing a role. This is now being investigated. Additionally, in all western blots, comparison of the two cell types consistently revealed CBS migrating as a doublet, with the lower band predominate in the ATM(−/−) cells and the upper band predominant in the ATM(+/+) cells (Fig. 3B and C). The significance of this in unknown but implies an ATM expression dependent post-translational CBS modification. This is also currently under investigation.

Previously low and dysregulated GSH metabolism was identified in A-T cells, A-T patients, and *Atm*-deficient mice, while treatment of A-T cells with NAC restored cellular GSH levels [23-25,30,31]. As A-T is characterized by increased ROS, low GSH, and increased genomic instability, we examined the effect of ATM expression on the GSH: GSSG ratio and the effects of exogenous NAC supplementation on ATM(−/−) and ATM(+/+) cell oxidative stress-induced dsDNA break formation [6-10,23-25]. Here we found that ATM expression significantly increased the GSH: GSSG ratio, while NAC reduced oxidative stress-induced dsDNA breaks in the ATM(−/−), but not the ATM (+/+) cells. Previously glutathione reductase activity was found to be low in *Atm*-deficient mice compared to wild-type mice [23]. Likely, ATM expression increased glutathione reductase activity, increasing the GSH: GSSG ratio. NAC reduced oxidative stress-induced dsDNA breaks in the ATM(−/−) cells only. The molecular mechanism for this is unknown, although it does indicate that dysregulated GSH metabolism in A-T cells contributes to their genomic instability. Low mitochondrial GSH results in lower Fe-S cluster stability and synthesis, and Fe-S cluster proteins are involved in DNA repair [28,29,32]. Possibly low A-T cell mitochondrial GSH results in low Fe-S cluster synthesis and subsequent poor A-T cell DNA repair. These hypotheses are being examined. Lastly, vector transduced ATM is known to undergo rearrangements, with these rearrangements often resulting in non-functioning or poorly functioning ATM proteins [26,59-61]. The ATM protein in the ATM(+/+) cells migrated at the molecular weight full-length of ATM and has previously been shown to function similarly to wild-type ATM [26]. Additionally, comparison of the ATM wild-type VA13 cell line to the A-T AT22 cell line revealed a similar ALS fraction increase seen in the ATM(+/+) cells. Based on this, the results presented here and previous data on primary A-T, ATM(−/−), ATM(+/+), and wild-type cell responses to iron chelators and labile iron, ATM plays a role in the regulation of Fe-S cluster synthesis, partially through NFS1 and NFU1 regulation [7-10]. The experiments here are being repeated in primary cells with siRNA-mediated ATM knockdown to confirm and extend these results.

Here we demonstrate that ATM regulates; 1) ALS fraction formation, 2) the cellular GSH: GSSG ratio, 3) the expression of CSE and CBS, 4) CSE activity, 5) Fe-S cluster complex I proteins NDUFS2, − 3, − 7, − 8, and succinate dehydrogenase expression, and 6) NFS1 and NFU1 protein expression. The data presented here indicates that ATM, like ATR, plays a role in regulating the cellular sulfide pool, especially as related to Fe-S cluster synthesis and GSH metabolism. Further work, including analyses of primary cell with ATM ablation and techniques such as electron paramagnetic resonance spectroscopy are underway to further define the exact function of ATM in Fe-S cluster synthesis and regulation.

Acknowledgements

This work was supported by funding from *The A-T Children's Project*. These studies were also supported by an Institutional Development Award (IDeA) from the National Institutes of General Medical Sciences of the National Institutes of Health under grant number P20GM121307 and National Institutes of Health grant numbers HL149264 (CGK) and HL139755 (CBP).

References

[1]. Savitsky K, Bar-Shira A, Gilad S, Rotman G, Ziv Y, Vanagaite L, Tagle DA, Smith S, Uziel T, Sfez S, A single ataxia telangiectasia gene with a product similar to PI-3 kinase, Science 268 (1995) 1749–1753, 10.1126/science.7792600. [PubMed: 7792600]

[2]. Keith CT, Schreiber SL, PIK-related kinases: DNA repair, recombination, and cell cycle checkpoints, Science 270 (1995) 50–51, 10.1126/science.270.5233.50. [PubMed: 7569949]

[3]. Imseng S, Aylett CH, Maier T, Architecture and activation of phosphatidylinositol 3-kinase related kinases, Curr. Opin. Struct. Biol 49 (2018) 177–189, 10.1016/j.sbi.2018.03.010. [PubMed: 29625383]

[4]. Matsuoka S, Ballif BA, Smogorzewska A, McDonald ER, Hurov KE, Luo J, Bakalarski CE, Zhao Z, Solimini N, Lerenthal Y, Shiloh Y, Gygi SP, Elledge SJ, ATM and ATR substrate analysis reveals extensive protein networks responsive to DNA damage, Science 316 (2007) 1160–1166, 10.1126/science.1140321. [PubMed: 17525332]

[5]. Kim ST, Lim DS, Canman CE, Kastan MB, Substrate specificities and identification of putative substrates of ATM kinase family members, J. Biol. Chem 274 (1999) 37538–37543, 10.1074/jbc.274.53.37538. [PubMed: 10608806]

[6]. Rothblum-Oviatt C, Wright J, Lefton-Greif MA, McGrath-Morrow SA, Crawford TO, Howard HM, Ataxia telangiectasia: a review, Orphanet J. Rare Dis 25 (2016) 159, 10.1186/s13023-016-0543-7.

[7]. Shackelford RE, Manuszak RP, Johnson CD, Hellrung DJ, Steele TA, Link CJ, Wang S, Desferrioxamine treatment increases the genomic stability of Ataxia-telangiectasia cells, DNA Repair 2 (2003) 971–981, 10.1016/S1568-7864(03)00090-9. [PubMed: 12967654]

[8]. Shackelford RE, Manuszak RP, Johnson CD, Hellrung DJ, Link CJ, Wang S, Iron chelators increase the resistance of Ataxia telangiectasia cells to oxidative stress, DNA Repair 2004 (3) (2004) 1263–1272, 10.1016/j.dnarep.2004.01.015.

[9]. Shackelford RE, Fu Y, Manuszak RP, Brooks TC, Sequeira AP, Wang S, Lowery-Nordberg M, Chen A, Iron chelators reduce chromosomal breaks in ataxia-telangiectasia cells, DNA Repair 2006 (5) (2006) 1327–1336, 10.1016/j.dnarep.2006.05.041.

[10]. Semlitsch M, Shackelford RE, Zirkl S, Sattler W, Malle E, ATM protects against oxidative stress induced by oxidized low-density lipoprotein, DNA Repair 10 (2011) 848–860, 10.1016/j.dnarep.2011.05.004. [PubMed: 21669554]

[11]. McDonald CJ, Ostini L, Wallace DF, John AB, Watters DJ, Subramaniam VN, Iron loading and oxidative stress in the Atm−/− mouse liver, Am. J. Physiol. Gastrointest. Liver Physiol 300 (2011) G554–G560, 10.1152/ajpgi.00486.2010. [PubMed: 21292994]

[12]. Xiao Q, Ying J, Xiang L, Zhang C, The biologic effect of hydrogen sulfide and its function in various diseases, Medicine 97 (2018), e13065, 10.1097/MD.0000000000013065. [PubMed: 30383685]

[13]. Rajendran S, Shen X, Glawe J, Kolluru GK, Kevil CK, Nitric oxide and hydrogen sulfide regulation of ischemic vascular growth and remodeling, Compr. Physiol 9 (2019) 1213–1247, 10.1002/cphy.c180026. [PubMed: 31187898]

[14]. Hellmich MR, Szabo C, Hydrogen sulfide and cancer, Handb. Exp. Pharmacol 230 (2015) 233–241, 10.1007/978-3-319-18144-8_12. [PubMed: 26162838]

[15]. Shackelford R, Ozluk E, Islam MZ, Hopper B, Meram A, Ghali G, Kevil CG, Hydrogen sulfide and DNA repair, Redox Biol. 38 (2021), 101675, 10.1016/j.redox.2020.101675. [PubMed: 33202302]

[16]. Rajpal S, Katikaneni P, Deshotels M, Pardue S, Glawe J, Shen X, Akkus N, Modi K, Bhandari R, Dominic P, Reddy P, Kolluru GK, Kevil CG, Total sulfane sulfur bioavailability reflects ethnic and gender disparities in cardiovascular disease, Redox Biol. 15 (2018) 480–489, 10.1016/j.redox.2018.01.007. [PubMed: 29413960]

[17]. Shen X, Peter EA, Bir S, Wang R, Kevil CG, Analytical measurement of discrete hydrogen sulfide pools in biological specimens, Free Radic. Biol. Med 52 (2015) 2276–2283, 10.1016/j.freeradbiomed.2012.04.007.

[18]. Shen X, Kolluru GK, Yuan S, Kevil CG, Measurement of H_2S in vivo and in vitro by the monobromobimane method, Methods Enzym. 554 (2015) 31–45, 10.1016/bs.mie.2014.11.039.

[19]. Ishigami M, Hiraki K, Umemura K, Ogasawara Y, Ishii K, Kimura H, A source of hydrogen sulfide and a mechanism of its release in the brain, Antioxid. Redox Signal 11 (2009) 205–214, 10.1089/ars.2008.2132. [PubMed: 18754702]

[20]. Chen J, Shen X, Pardue S, Meram AT, Rajendran S, Ghali GE, Kevil CG, Shackelford RE, The *Ataxia telangiectasia-mutated* and Rad3-related protein kinase regulates cellular hydrogen sulfide concentrations, DNA Repair 73 (2019) 55–63, 10.1016/j.dnarep.2018.11.002. [PubMed: 30470507]

[21]. Durocher D, Jackson SP, DNA-PK ATM and ATR as sensors of DNA damage: variations on a theme? Curr. Opin. Cell Biol 13 (2001) 225–231, 10.1016/s0955-0674(00)00201-5. [PubMed: 11248557]

[22]. Hanawalt PC, Historical perspective on the DNA damage response, DNA Repair 36 (2015) 2–7, 10.1016/j.dnarep.2015.10.001. [PubMed: 26507443]

[23]. Meredith MJ, Dodson ML, Impaired glutathione biosynthesis in cultured human ataxia-telangiectasia cells, Cancer Res. 47 (1987) 4576–4581. [PubMed: 3621155]

[24]. Campbell A, Bushman J, Munger J, Noble M, Pröschel C, Mayer-Pröschel M, Mutation of ataxia-telangiectasia mutated is associated with dysfunctional glutathione homeostasis in cerebellar astroglia, Glia 64 (2016) 227–239, 10.1002/glia.22925. [PubMed: 26469940]

[25]. Andrade IGA, Isabel Suano-Souza F, Luiz F, Fonseca A, Aranda Lago CS, Sarni ROS, Selenium levels and glutathione peroxidase activity in patients with ataxia-telangiectasia: association with oxidative stress and lipid status biomarkers, Orphanet J. Rare Dis 16 (2021) 83, 10.1186/s13023-021-01732-5. [PubMed: 33579341]

[26]. Ziv Y, Bar-Shira A, Pecker I, Russell P, Jorgensen TJ, Tsarfati I, Shiloh Y, Recombinant ATM protein complements the cellular A-T phenotype, Oncogene 15 (1997) 159–167, 10.1006/prep.2001.1459. [PubMed: 9244351]

[27]. Kolluru GK, Bir SC, Yuan S, Shen X, Pardue S, Wang R, Kevil CG, Cystathionine gamma-lyase regulates arteriogenesis through NO-dependent monocyte recruitment, Cardiovasc. Res 107 (2015) 590–600, 10.1093/cvr/cvv198. [PubMed: 26194202]

[28]. Braymer JJ, Lill R, Iron-sulfur cluster biogenesis and trafficking in mitochondria, J Biol Chem 292 (20171) 12754–12763. 10.1074/jbc.R117.787101. [PubMed: 28615445]

[29]. Wang Y, Yen FS, Zhu XG, Timson RC, Weber R, Xing C, Liu Y, Allwein B, Luo H, Yeh HW, Heissel S, Unlu G, Gamazon ER, Kharas MG, Hite R, Birsoy K, SLC25A39 is necessary for mitochondrial glutathione import in mammalian cells, Nature 599 (2021) 136–140, 10.1038/s41586-021-04025-w. [PubMed: 34707288]

[30]. Reliene R, Fleming SM, Chesselet MF, Schiesti RH, Effects of antioxidants on cancer prevention and neuromotor performance in Atm deficient mice, Food Chem. Toxicol 46 (2008) 1371–1377, 10.1016/j.fct.2007.08.028. [PubMed: 18037553]

[31]. Ruffmann R, Wendel A, GSH rescue by N-acetylcysteine, Klin. Woche 69 (1991) 857–862, 10.1007/BF01649460.

[32]. Johnson DC, Dean DR, Smith AD, Johnson MK, Structure, function, and formation of biological iron-sulfur clusters, Ann Rev Biochem 74 (205) 247–281. https://doi: (10.1146/annurev.biochem.74.082803.133518).

[33]. Chen PH, Wu J, Ding CC, Lin CC, Pan S, Bossa N, Xu Y, Yang WH, Mathey-Prevot B, Chi JT, Kinome screen of ferroptosis reveals a novel role of ATM in regulating iron metabolism, Cell Death Differ. 27 (2020) 1008–1022, 10.1038/s41418-019-0393-7. [PubMed: 31320750]

[34]. Biederbick A, Stehling O, Rösser R, Niggemeyer B, Nakai Y, Elsässer HP, Lill R, Role of human mitochondrial Nfs1 in cytosolic iron-sulfur protein biogenesis and iron regulation, Mol. Cell Biol 26 (2006) 5675–5687, 10.1128/MCB.00112-06. [PubMed: 16847322]

[35]. Farhan SMK, Wang J, Robinson JF, Lahiry P, Siu VM, Prasad C, Kronick JB, Ramsay DA, Rupar CA, Hegele RA, Exome sequencing identifies *NFS1* deficiency in a novel Fe-S cluster disease, infantile mitochondrial complex II/III deficiency, Mol. Genet. Genom. Med 2 (2014) 73–80, 10.1002/mgg3.46.

[36]. Hershkovitz T, Kurolap A, Tal G, Paperna T, Mory A, Staples J, Brigatti Karlla W., Gonzaga-Jauregui C, Dumin E, Saada A, Mandel H, Feldman HB, A recurring *NFS1* pathogenic variant causes a mitochondrial disorder with variable intra-familial patient outcomes, Mol. Genet Metab. Rep 26 (2021), 100699, 10.1016/j.ymgmr.2020.100699. [PubMed: 33457206]

[37]. Navarro-Sastre A, Tort F, Stehling O, Uzarska MA, Arranz JA, Del Toro M, Teresa Labayru M, Landa J, Font A, Garcia-Villoria J, Merinero B, Ugarte M, Gutierrez-Solana LG, Campistol J, Garcia-Cazorla A, Vaquerizo J, Riudor E, Briones P, Elpeleg O, Ribes A, Lill R, A fatal mitochondrial disease is associated with defective NFU1 function in the maturation of a subset of mitochondrial Fe-S proteins, Am. J. Hum. Genet 89 (2011) 656–667, 10.1016/j.ajhg.2011.10.005. [PubMed: 22077971]

[38]. GeneCards®: The Human Gene Database, (http://www.genecards.org), accessed for NFS1 and NFU1, 4/25/2022.

[39]. Zhang J, Chen GQ, Hypoxia-HIF-1alpha-C/EBPalpha/Runx1 signaling in leukemic cell differentiation, Pathophysiology 16 (2009) 297–303, 10.1016/j.pathophys.2009.02.005. [PubMed: 19285840]

[40]. Mongiardi MP, Stagni V, Natoli M, Giaccari D, D'Agnano I, Falchetti ML, Barilà D, Levi A, Oxygen sensing is impaired in ATM-defective cells, Cell Cycle 10 (2011) 4311–4320, 10.4161/cc.10.24.18663. [PubMed: 22134239]

[41]. Blignaut M, Loos B, Botchway SW, Parker AW, Huisamen B, Ataxia-Telangiectasia mutated is located in cardiac mitochondria and impacts oxidative phosphorylation, Sci. Rep 9 (2019) 4781, 10.1038/s41598-019-41108-1. [PubMed: 30886207]

[42]. Haack TB, Haberberger B, Frisch EM, Wieland T, Iuso A, Gorza M, Strecker V, Graf D, Mayr JA, Herberg U, Hennermann JB, Klopstock T, Kuhn KA, Ahting U, Sperl W, Wilichowski E, Hoffmann GF, Tesarova M, Hansikova H, Zeman J, Plecko B, Zeviani M, Wittig I, Strom TM, Schuelke Ms, Freisinger P, Meitinger T, Prokisch H, Molecular diagnosis in mitochondrial complex I deficiency using exome sequencing, J. Med. Genet 49 (2012) 277–283, 10.1136/jmedgenet-2012-100846. [PubMed: 22499348]

[43]. Dunham-Snary KJ, Wu D, Potus F, Sykes EA, Mewburn JD, Charles RL, Eaton P, Sultanian RA, Archer SL, Ndufs2, a core subunit of mitochondrial complex I, is essential for acute oxygen-sensing and hypoxic pulmonary vasoconstriction, Circ. Res 2019 (124) (2019) 1727–1746, 10.1161/CIRCRESAHA.118.314284.

[44]. Lebon S, Rodriguez D, Bridoux D, Zerrad A, Rötig A, Munnich A, Legrand A, Slama A, A novel mutation in the human complex I NDUFS7 subunit associated with Leigh syndrome, Mol. Genet. Metab 90 (2007) 379–382, 10.1016/j.ymgme.2006.12.007. [PubMed: 17275378]

[45]. Valentin-Vega YA, MacLean KH, Tait-Mulder J, Milasta S, Steeves M, Dorsey FC, Cleveland JL, Green DR, Kastan MB, Mitochondrial dysfunction in ataxia-telangiectasia, Blood 119 (2012) 1490–1500, 10.1182/blood-2011-08-373639. [PubMed: 22144182]

[46]. Fassone E, Rahman S, Complex I deficiency: clinical features, biochemistry and molecular genetics, J. Med. Genet 49 (2014) 578–590, 10.1136/jmedgenet-2012-101159.

[47]. Wiley SE, Paddock ML, Abresch EC, Gross L, van der Geer P, Nechushtai PR, Murphy AN, Jennings PA, Dixon JE, The outer mitochondrial membrane protein mitoNEET contains a novel redox-active 2Fe-2S cluster, J. Biol. Chem 282 (2007) 23745–23749, 10.1074/jbc.C700107200. [PubMed: 17584744]

[48]. Benit P, Slama A, Cartault F, Giurgea I, Chretien D, Lebon S, Marsac C, Munnich A, Roetig A, Rustin P, Mutant NDUFS3 subunit of mitochondrial complex I causes Leigh syndrome, J. Met. Genet 41 (2004) 14–17, 10.1136/jmg.2003.014316.

[49]. Lebon S, Rodriguez D, Bridoux D, Zerrad A, Roetig A, Munnich A, Legrand A, Slama A, A novel mutation in the human complex I NDUFS7 subunit associated with Leigh syndrome, Mol. Genet. Metab 90 (2007) 379–382, 10.1016/j.ymgme.2006.12.007. [PubMed: 17275378]

[50]. Dunham-Snary KJ, Wu D, Potus F, Sykes EA, Mewburn JD, Charles RL, Eaton P, Sultanian RA, Archer SL, Ndufs2, a core subunit of mitochondrial complex I, is essential for acute oxygen-sensing and hypoxic pulmonary vasoconstriction, Circ. Res 124 (2009) 1727–1746, 10.1161/CIRCRESAHA.118.314284.

[51]. Loeffen J, Smeitink J, Triepels R, Smeets R, Schuelke M, Sengers R, Trijbels F, Hamel B, Mullaart R, van den Heuvel L, The first nuclear-encoded complex I mutation in a patient with Leigh syndrome, Am. J. Hum. Genet 63 (1998) 1598–1608, 10.1086/302154. [PubMed: 9837812]

[52]. Amr S, Heisey C, Zhang M, Xia XJ, Shows KH, Ajlouni K, Pandya A, Satin LS, El-Shanti H, Shiang R, A homozygous mutation in a novel zinc-finger protein, ERIS, is responsible for Wolfram syndrome 2, Am. J. Hum. Genet 81 (2007) 673–683, 10.1086/520961. [PubMed: 17846994]

[53]. Chen YF, Wu CY, Kirby R, Kao CH, Tsai TF, A role for the CISD2 gene in lifespan control and human disease. Ann N Y Acad Sci 1201 (2110) 58–64. doi:10.1111/j.1749-6632.2010.05619.x.

[54]. Kanki T, Klionsky DJ, Mitochondrial abnormalities drive cell death in Wolfram syndrome 2, Cell Res. 19 (2009) 922–923, 10.1038/cr.2009.94. [PubMed: 19648948]

[55]. Zhang P, Wei Y, Wang L, Debeb BD, Yuan Y, Zhang J, Yuan J, Wang M, Chen D, Sun Y, Woodward WA, Liu Y, Dean DC, Liang H, Hu Y, Ang KK, Hung MC, Chen J, Ma L, ATM-mediated stabilization of ZEB1 promotes DNA damage response and radioresistance through CHK1, Nat. Cell Biol 16 (2014) 864–875, 10.1038/ncb3013. [PubMed: 25086746]

[56]. Ui A, agaura Y, Yasui A, Transcriptional elongation factor ENL phosphorylated by ATM recruits polycomb and switches off transcription for DSB repair, Mol. Cell 58 (2015) 468–482, 10.1016/j.molcel.2015.03.023. [PubMed: 25921070]

[57]. Crooks DR, Maio N, Lane AN, Jarnik M, Higashi RM, Haller RG, Yang Y, Fan TW-M, Linehan WM, Rouault TA, Acute loss of iron-sulfur clusters results in metabolic reprogramming and generation of lipid droplets in mammalian cells, J. Biol. Chem 293 (2018) 8297–8311, 10.1074/jbc.RA118.001885. [PubMed: 29523684]

[58]. Donath H, Woelke S, Theis M, Heß U, Knop V, Herrmann E, Krauskopf D, Kieslich M, Schubert R, Zielen S, Progressive liver disease in patients with Ataxia telangiectasia, Front. Pediatr 7 (2019) 458, 10.3389/fped.2019.00458. [PubMed: 31788461]

[59]. Oguchi K, Takagi M, Tsuchida R, Taya Y, Ito E, Isoyama K, Ishii E, Zannini L, Delia D, Mizutani S, Missense mutation and defective function of ATM in a childhood acute leukemia patient with MLL gene rearrangement, Blood 101 (2003) 3622–3627, 10.1182/blood-2002-02-0570. [PubMed: 12511424]

[60]. Stoppa-Lyonnet D, Soulier J, Laugé A, Dastot H, Garand R, Sigaux F, Stern MH, Inactivation of the ATM gene in T-cell prolymphocytic leukemias, Blood 91 (1998) 3920–3926, 10.1182/blood.V91.10.3920. [PubMed: 9573030]

[61]. Kanagal-Shamanna R, Bao H, Kearney H, Smoley S, Tang Z, Luthra R, Yang H, Zhang S, Lin P, Wu D, Medeiros LJ, Lu X, Molecular characterization of Novel *ATM* fusions in chronic lymphocytic leukemia and T-cell prolymphocytic leukemia, Leuk. Lymphoma (2021) 1–11, 10.1080/10428194.2021.2010061.

[62]. Gutscher M, Pauleau AL, Marty L, Brach T, Wabnitz GH, Samstag Y, Meyer AJ, Dick TP, Real-time imaging of the intracellular glutathione redox potential, Nat. Methods 5 (6) (2008) 553–559, 10.1038/nmeth.1212. [PubMed: 18469822]

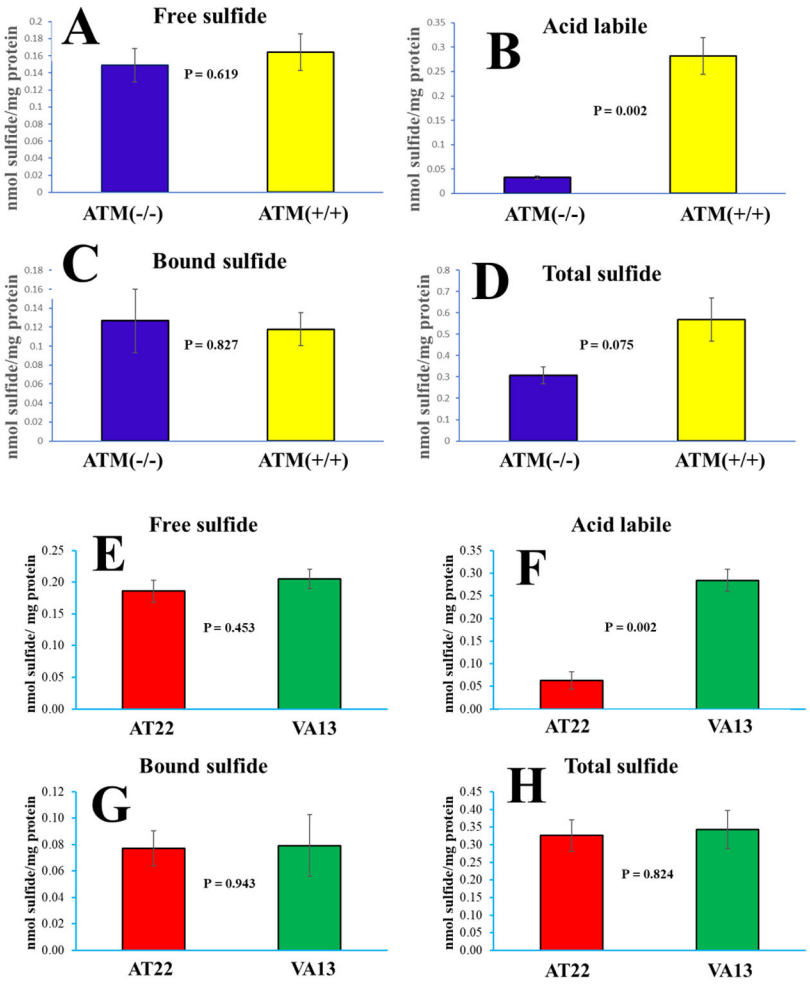

Fig. 1.

Free H_2S (A and E), the acid-labile (B and F), bound sulfane (C and G), and total sulfide fractions (D and H) were determined in the ATM(−/−), ATM(+/+), AT22, and VA13 cells by the MBB method [16-18,20]. The ATM(−/−) cells are in blue, ATM(+/+) cells are in yellow, the AT22 cells are in red, and the VA13 cells are in green.

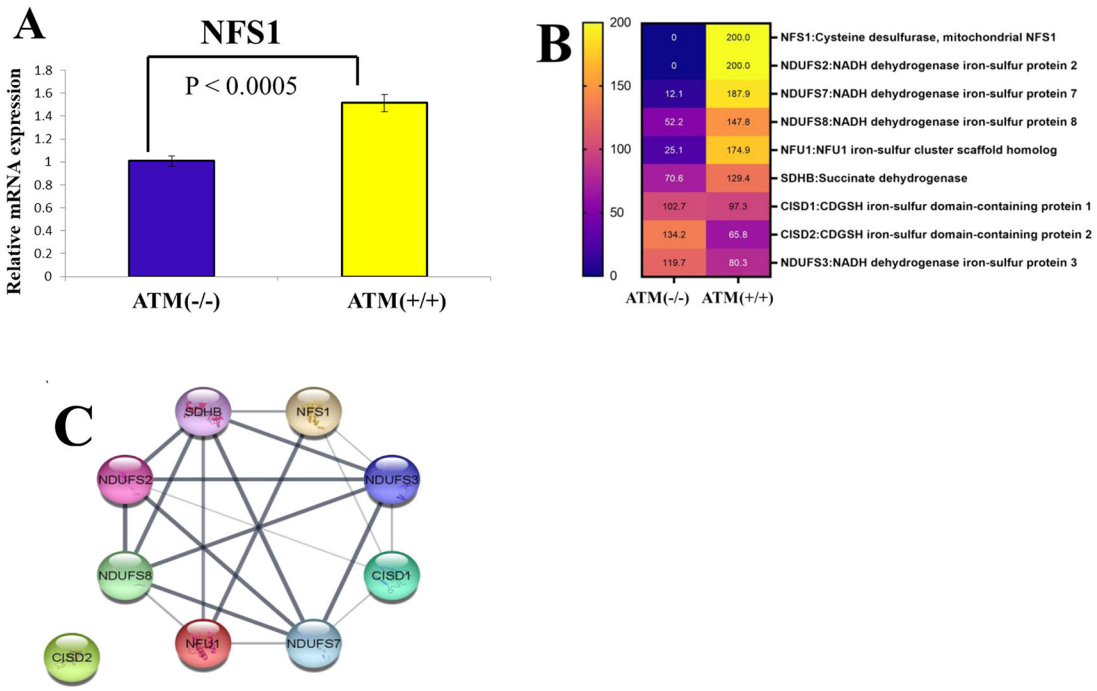

Fig. 2.

The mRNA expression levels of NFS1 in ATM(−/−) and ATM+ /+) cells. The ATM(−/−) cells are in blue and the ATM(+/+) cells are in yellow (A). Proteomics Heatmap of the ATM(−/−) and ATM(+/+) cells (B). Yellow represents elevated expression levels and blue represents lower expression levels. Visualization of the protein-protein interaction of Fe-S proteins and cysteine desulfurase using STRING and Cytoscape databases (C).

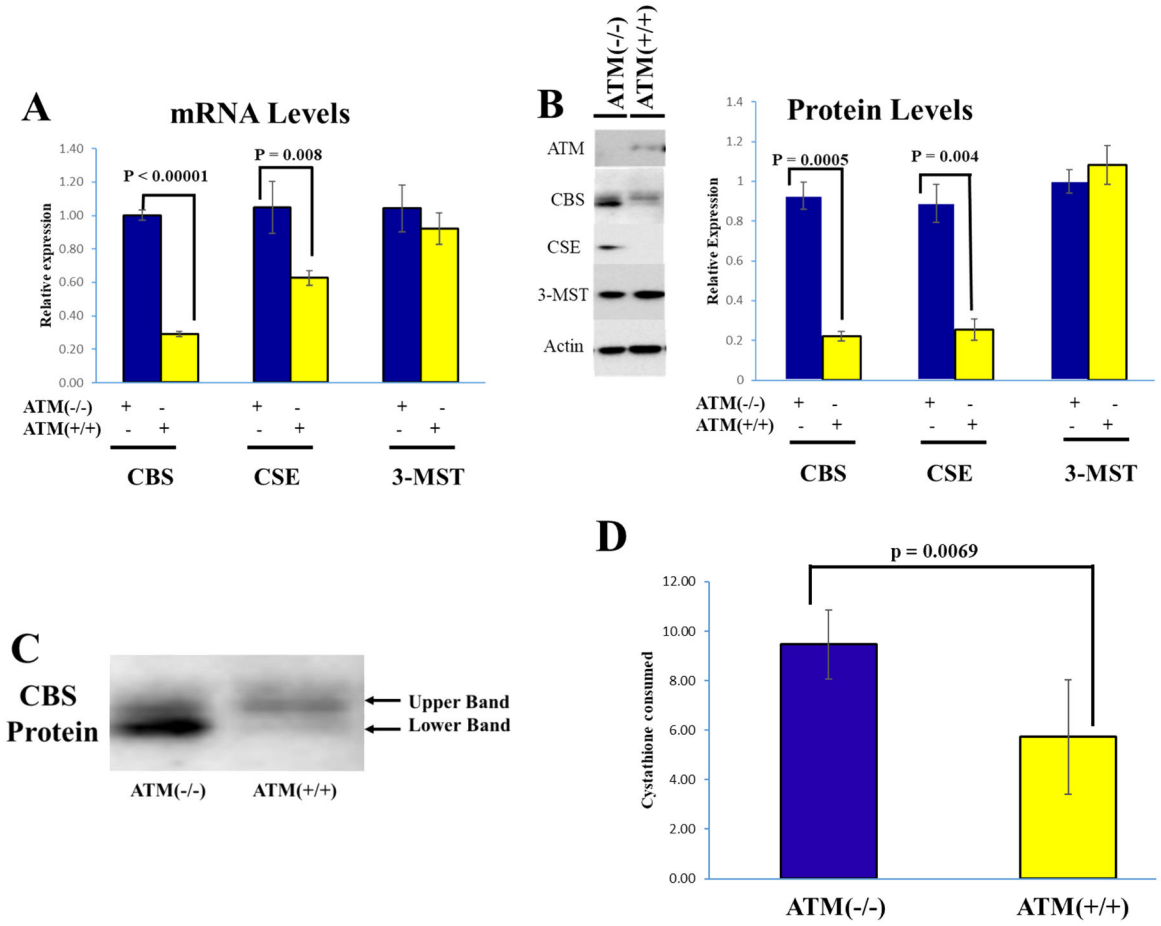

Fig. 3.

The mRNA (A) and protein levels (B) of CBS, CSE, and 3-MST were compared in the ATM(−/−) and ATM(+/+) cells. Panel C depicts the expanded doublet staining pattern seen in the CBS western blot, without and with ATM expression. CSE enzymatic activity was similarly compared between the ATM(−/−) and the ATM(+/+) cells (D). CSE activity was analyzed by cystathionine consumption and enzyme activity as fold change calculated for nmol cystathionine consumed per total protein [27]. The ATM(−/−) cells are in blue, and the ATM(+/+) cells are in yellow.

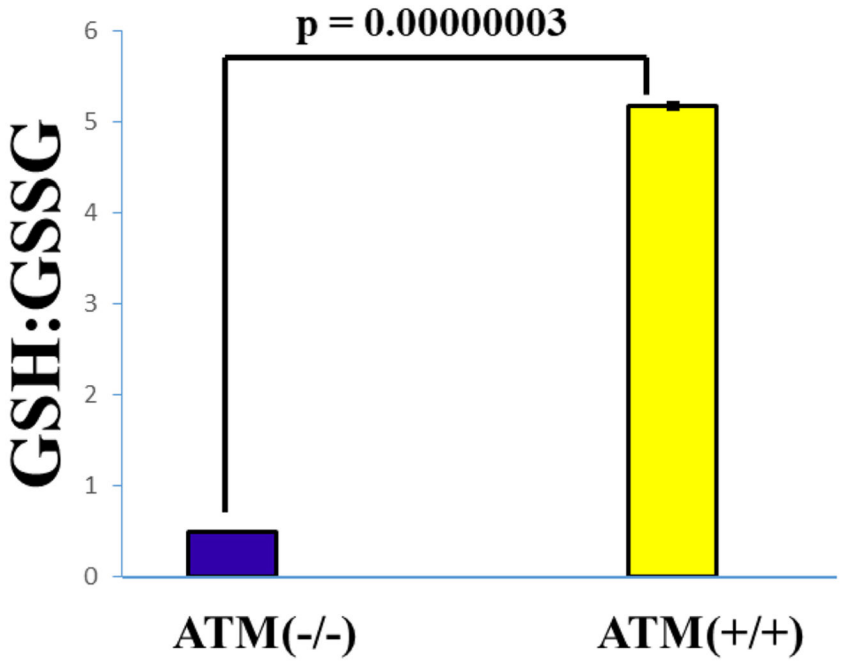

Fig. 4.

The relative GSH: GSSG ratio in ATM(−/−) cells compared to the ATM+ /+) cells. The ATM(−/−) cells are in blue, and the ATM+ /+) cells are in yellow.

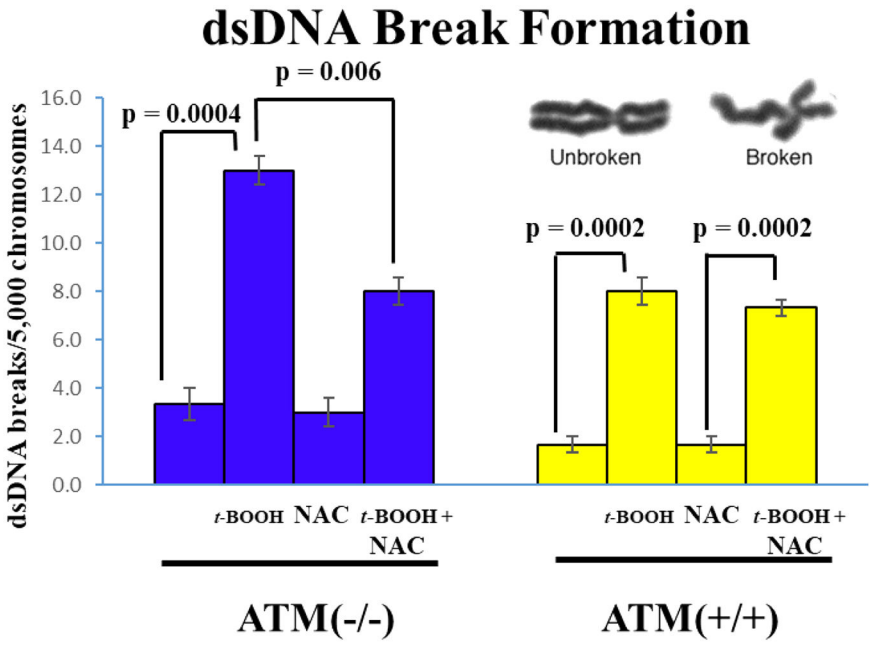

Fig. 5.

ATM(−/−) and ATM(+/+) cell dsDNA breaks were analyzed in under oil immersion microscopy of colcemid-blocked, Giemsa stained chromosomal preparations, without and with *t*-BOOH and NAC exposures [20]. [*t*-BOOH] was 10 μM and [NAC] was 30 μM. The ATM(−/−) cells are in blue, and the ATM(+/+) cells are in yellow. Examples of intact and broken chromosomes with a dsDNA break are shown in the insert.

Table 1

Forward and reverse primers used to quantify GAPDH, CBS, CSE, and 3-MST mRNA expression in the ATM(−/−) and ATM(+/+) cell lines. GAPDH primers were employed for control normalization of the genes examined.

Gene	Species	Forward	Reverse
GAPDH	**Human**	ACAGTCAGCCGCATCTTC	CGCCCAATACGACCAAATC
CBS	**Human**	AGGATGAACACAGGCAAT	AAAAACCCAAACACGCAAAC
CSE	**Human**	GCCTTTGCTTCAGGTTTAGC	CCTTCTGGGTGGGGTTTGT
3-MST	**Human**	ACCGTGAACATCCCCTTC	TTCTTCTCCTGGAACAGATG
NFS1	**Human**	GGCTTGCCAGATGAGAAAGG	CCTCCAATTCAGCACCACTG

DNA Repair (Amst). Author manuscript; available in PMC 2024 May 24.

Table 2

Quantification of the free H_2S, acid-labile, bound, and total sulfide fractions in the ATM(−/−), ATM(+/+), AT22, and VA13 cells by the MBB method [16-18,20]. The sulfides are in nmols sulfide/mg protein. The SEMs are given in the table and are derived from triplicate measurements within each sulfide fraction.

Cell Type	Free H_2S (nmol sulfide/mg protein)	Acid-Labile Sulfide Fraction (nmol sulfide/ mg protein)	Bound Sulfide Fraction (nmol sulfide/ mg protein)	Total Sulfide Fraction (nmol sulfide/ mg protein)
ATM(−/−) Cells	0.14868 SEM= 0.020	0.03236 SEM= 0.004	0.12669 SEM= 0.033	0.10257 SEM= 0.041
ATM(+/+) Cells	0.16432 SEM= 0.022	0.28227 SEM= 0.038	0.11794 SEM= 0.017	0.18817 SEM= 0.102
AT22 A-T cell	0.18587 SEM= 0.017	0.06318 SEM= 0.019	0.07723 SEM= 0.013	0.326293 SEM= 0.044
VA13 ATM wild-type	0.20501 SEM= 0.015	0.284269 SEM= 0.024	0.07925 SEM= 0.023	0.34284 SEM= 0.054

Table 3

Quantification of the dsDNA breaks in the ATM(−/−) and ATM(+/+) cells without and with *t*-BOOH and NAC exposures. [*t*-BOOH] was 10 μM and [NAC] was 30 μM. The standard errors of the mean (SEM) are listed, and all counts were dsDNA breaks/5000 total chromosomes counted in triplicate [20].

Cell Type and Treatment	Average dsDNA breaks/5000 chromosomes	SEM
ATM(−/−) Cells	2.67	0.54
ATM(−/−) Cells + *t*-BOOH	13.0	0.47
ATM(−/−) Cells + NAC	3.0	0.47
ATM(−/−) Cells + NAC + *t*-BOOH	8.0	0.47
ATM(+/+) Cells	1.67	0.27
ATM(+/+) Cells + *t*-BOOH	8.0	0.47
ATM(+/+) Cells + NAC	1.67	0.27
ATM(+/+) Cells + NAC + *t*-BOOH	7.33	0.27